Hindawi
Journal of Nanomaterials
Volume 2021, Article ID 4702995, 12 pages
https://doi.org/10.1155/2021/4702995

Research Article

Preparation of Electrode Material Based to Bismuth Oxide-Attached Multiwalled Carbon Nanotubes for Lead (II) Ion Determination

Hai D. Tran,[1] **Anh H. Q. Le**,[1] **and Uyen P. N. Tran**[2]

[1] *Ho Chi Minh City University of Natural Resources and Environment, Ho Chi Minh City 700000, Vietnam*
[2] *Van Hien University, Ho Chi Minh City 700000, Vietnam*

Correspondence should be addressed to Hai D. Tran; tdhai@hcmunre.edu.vn and Uyen P. N. Tran; uyentpn@vhu.edu.vn

Received 11 May 2021; Revised 5 August 2021; Accepted 31 August 2021; Published 25 October 2021

Academic Editor: Mazeyar Parvinzadeh Gashti

Bi_2O_3 was proven an attractive compound for electrode modification in heavy metal electrochemical analysis. A novel method for synthesizing Bi_2O_3-attached multiwalled carbon nanotubes (Bi_2O_3@CNTs) in solution is successfully developed in this study. Characteristics of the obtained Bi_2O_3@CNTs were proven by modern techniques such as X-ray diffraction, Raman spectroscopy, scanning electronic microscopy, transmission electron microscopy, cyclic voltammetry, electrochemical impedance spectroscopy, and anodic stripping voltammetry. Microscopy images and spectra results reveal that Bi_2O_3 particles are mainly attached at defect points on multiwalled carbon nanotubes (MWCNTs) walls. Paste electrodes based on the MWCNTs and synthesized Bi_2O_3@CNTs were applied for electrochemical measurements. The redox mechanism of Bi_2O_3 on the electrode surface was also made clear by the cyclic voltammetric tests. The recorded cyclic voltammograms and electrochemical impedance spectroscopy demonstrate that the Bi_2O_3@CNTs electrode was in lower charge transfer resistance than the CNTs one and in the controlled diffusion region. Investigation on the electrochemical behavior of Pb^{2+} at the Bi_2O_3@CNTs electrodes found a significant improvement of analytical response, resulting in 3.44 μg/L of the detection limit and 2.842 μA/(μg/L) of the sensitivity with linear sweep anodic stripping voltammetry technique at optimized conditions.

1. Introduction

Currently, researchers are focusing on controlling the level of heavy metals in waterways through developing novel sensors for detecting heavy metals such as lead. As low concentrations of lead (II) can cause severe ecological damage and harm human health (such as anemia, weakness, and kidney and brain damage) [1], developing a fast and highly efficient method for accurately detecting lead in wastewater is extremely necessary. Anodic stripping voltammetry (ASV) is a powerful, sensitive and selective electrochemical technique for determining heavy metal ions such as Pb [1]. These ionic species are first deposited on the working electrode (WE) in the accumulation step under a reduction potential. Followed by a potential scan, the analyte is stripped back into the solution in the stripping step, resulting in a current response proportional to its concentration [2, 3]. These redox processes occur on the WE surface, where mass and electrons are transported, and these processes depend significantly on the properties of the electrode material.

Existing literature provides an overview of several suitable electrochemical materials for WE construction [4]. Although the traditional mercury electrode has advantages, replacing it with other suitable materials is necessary owing to its toxicity to humans and the environment [5, 6]. Advanced carbon forms have been considered promising electrode replacements as they are ecofriendly and exhibit excellent electrical conductivity, chemical stability, structural versatility, and broad potential windows [3]; moreover, they require simple modifications for their application as electrodes. Carbon nanotubes (CNTs) [7], graphene [8], graphene oxide [9], and carbon nanofibers [10] are extremely useful as carbon paste electrodes to trace heavy metals from different sources. The sensing applications of MWCNTs are being developed due to several useful properties such as large surface area, fast electric signal transport, and functionability [11, 12]. The highly porous structure of nanocarbons generates a thick double layer and stable film on the WE surface [13] that are detrimental to metal detection [13, 14]. Therefore, these carbon materials must be modified to overcome these drawbacks.

In the presence of Bi on the WE surface, multicomponent alloys of Bi^0 and heavy metals are formed during the accumulation step [15], resulting in improved efficiency and sensitivity [16]. Most recent methods to prepare Bi-film-coated electrodes are based on ex situ, in situ, or bulk modification with different Bi compounds [17]. However, these approaches have certain disadvantages [18]. The pH of the solution on the WE surface (interface) is an important parameter affecting the existing forms of bismuth and heavy metal ions [17, 18]. However, proton changes (release or consumption) in the cathodic and anodic processes can vary the pH [19], thereby influencing the repeatability and reproducibility of the Bi-film-coated electrode [20]. In another study, Bi_2O_3 was applied as a bulk modifier, mixed with carbon for electrode fabrication to improve heavy metal detection [17]. In a weakly acidic electrolyte, the Bi film on the WE surface is formed owing to the reduction of Bi^{3+} in Bi_2O_3 to Bi^0 under an appropriate potential.

This study is aimed at developing a new method for preparing Bi_2O_3-attached multiwalled carbon nanotubes (Bi_2O_3@CNTs) for paste electrode construction. The Bi_2O_3@CNTs were prepared using ultrasonication to effectively disperse Bi on the outer walls of CNTs, resulting in a unique material for lead ion determination. The performance of the fabricated electrodes in detecting Pb^{2+} was analyzed using the ASV technique. This work paves the way to produce cost-effective and environment-friendly electrochemical sensors for monitoring heavy metal contamination in aquatic environments.

2. Experimental

2.1. Materials and Apparatus. Multiwalled carbon nanotubes synthesized through chemical vapor deposition were supplied by Vinanotech (Vietnam). Analytical grade Bi $(NO_3)_3{\cdot}5H_2O$ (>98%), $Pb(NO_3)_2$ (>99.95%), CH_3COOH (>99.7%), HNO_3 (~68%), NaOH (>99.9%), and $K_3Fe(CN)_6{\cdot}3H_2O$ (>99%) were purchased from Sigma-Aldrich (US). Paraffin oil and n-hexane were purchased from Merck (Germany). Double distilled water was used as the medium for preparing solutions.

X-ray diffraction (XRD) patterns of the materials were obtained via a Bruker D2 PHASER spectrometer using Cu Kα radiation of wavelength ($\lambda = 1.5406$ Å). Raman spectra were collected using a LabRAM HR Evolution spectroscopy with a 532 nm laser. The morphologies of the materials were examined using a field emission scanning electron microscope (FESEM S4800, Hitachi, Japan) and a transmission electron microscope (TEM, JEM-1400, Jeol, USA). Electrochemical experiments using a three-electrode cell at 25°C were performed with an MPG2 Biologic system (Biologic Sci. Ins., India) and controlled using the ECLab® software. A platinum grid, Ag/AgCl, and Bi_2O_3@CNTs electrodes were set up as the counter, reference, and working electrodes, respectively. Inductively coupled plasma-mass spectroscopy (ICP-MS) technique applying the US EPA method 200.8 for the validation of the ASV method was conducted by a 7800 ICP-MS instrument (Agilent, US).

2.2. Preparation of the Bi_2O_3@CNTs. Approximately 20 g CNTs was added to 1500 mL of HNO_3 (68%) in a flask, which was placed in an ultrasonic tank. The CNTs were dispersed and oxidized for 2 h at room temperature. The solid material was then collected by centrifugal separation. The obtained sediment was redispersed in water and transferred into a vacuum filtration system for filtration and washing until a neutral solution was obtained. These oxidized CNTs were dried overnight at 110°C and used for Bi_2O_3 attachment.

Next, 3 g of the oxidized CNTs was mixed with 50 mL of $Bi(NO_3)_3$ solution (20, 50, and 70 mmol/L), which was acidified using 5 mL of HNO_3 solution (0.1 M). Interactions between CNTs and Bi^{3+} occurred for 30 min under stirring. Next, NaOH solution (0.1 M) was slowly dropped into the mixture (at intervals of ~10 s) until the pH reached 6.5. Subsequently, the mixture was sonicated for 10 min. The solid was then filtrated and washed several times. The obtained materials were heated to 270°C and held for 2 h. The final products were labelled as Bi_2O_3@CNTs-20, Bi_2O_3@CNTs-50, and Bi_2O_3@CNTs-70, corresponding to concentrations of 20, 50, and 70 mmol/L of the used $Bi(NO_3)_3$ solution.

2.3. Electrode Fabrication. Mixtures of CNTs (or Bi_2O_3@CNTs) and paraffin oil (80 : 20 wt.%, respectively) were dispersed in n-hexane under ultrasonication until pastes were formed. The obtained fresh pastes were packed and pressed into the end of the cavity with a 3 mm inner diameter in the polytetrafluoroethylene (PTFE) electrode body. A copper wire was used to conduct electrical signals. The electrode surface was polished on a weigh paper before each electrochemical measurement.

2.4. Electrochemical Measurements. A solution mixture of 0.1 M KCl and 0.1 M acetate buffer (pH 4.0) was used as the electrolytic support for all electrochemical tests. The cyclic voltammetry (CV) measurements with the potential ranging from –0.2 V to 1.0 V at different scan rates (10, 20, 30, 40, 50, 70, 100, 150, and 200 mV/s) and electrochemical impedance spectroscopy (EIS) with a 5 mV amplitude over a frequency range of $1–10^5$ Hz were conducted on the electrodes in the electrolyte containing 50 mM $K_3Fe(CN)_6$.

The Pb^{2+} concentrations in the electrolyte were quantified using linear sweep anodic stripping voltammetry (LSASV). WE was first subjected to an accumulation potential (E_{acc}) for an accumulation time (t_{acc}) while the solution was stirred. Following the accumulation step, stirring was stopped to reach an equilibrium period of 10 s, and stripping voltammograms were recorded by sweeping the potential from E_{acc} to +0.2 V at a rate of 50 mV/s. The E_{acc}, t_{acc}, and pH of the electrolyte were optimized.

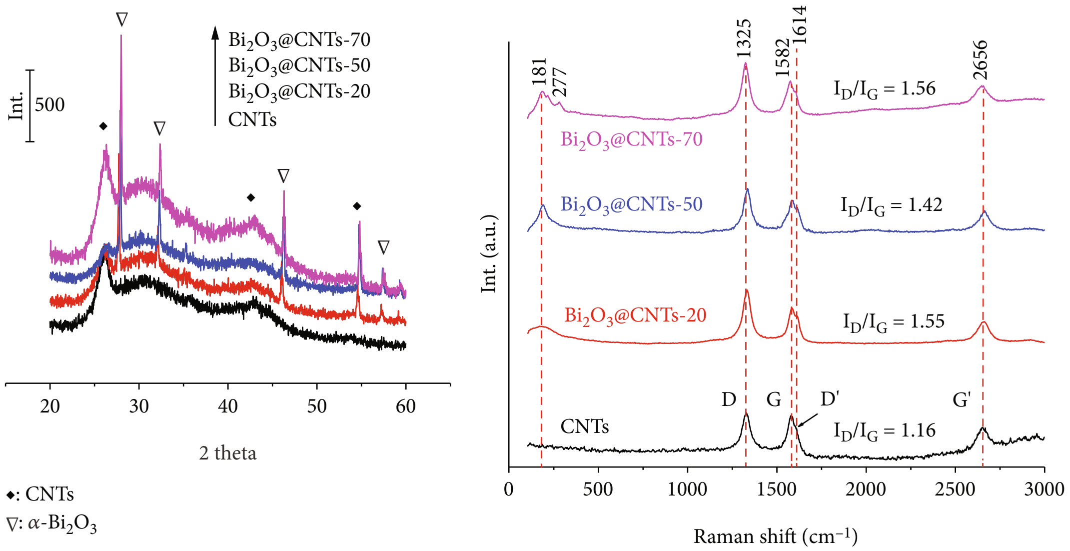

(a) (b)

Figure 1: (a) XRD patterns and (b) Raman spectra of CNTs and Bi$_2$O$_3$@CNTs.

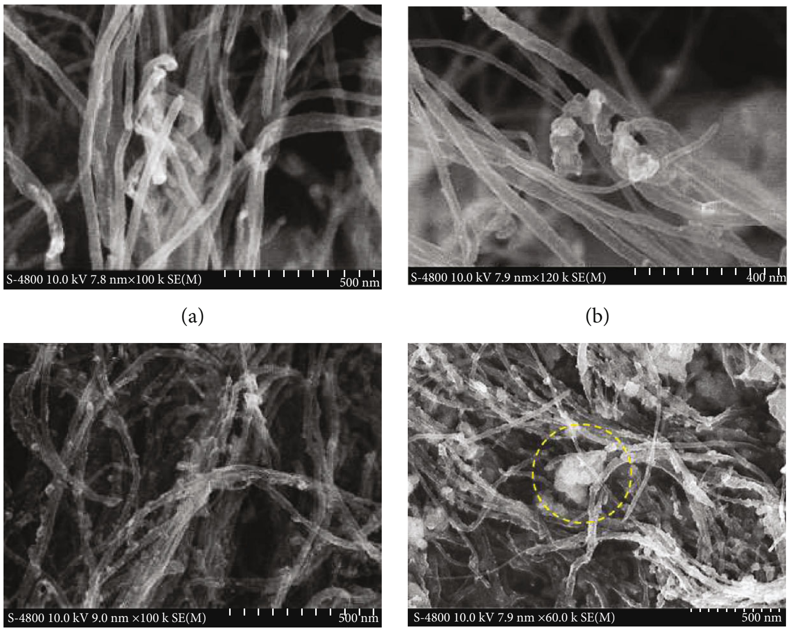

(a) (b)

(c) (d)

Figure 2: SEM images of (a) CNTs, (b) Bi$_2$O$_3$@CNTs-20, (c) Bi$_2$O$_3$@CNTs-50, and (d) Bi$_2$O$_3$@CNTs-70.

3. Results and Discussion

3.1. Characterization of Electrode Materials. Figure 1(a) presents the XRD patterns of the CNTs and Bi$_2$O$_3$@CNTs. The characteristic diffraction peaks of CNTs at $2\theta = 26.4^\circ$ and 43.2° were assigned to the C(100) and C(002) planes [21]. These two peaks indicate the existence of amorphous phases in the CNTs owing to their low intensity and large width [22]. The diffraction peaks for α-Bi$_2$O$_3$ are observed at $2\theta = 28.0^\circ$ (021), 32.3° (220), 46.3° (222), and 54.7° (023) in the XRD patterns of the Bi$_2$O$_3$@CNTs, corresponding to the JCPDS file no. 76-1730. These results indicate that the synthesized Bi$_2$O$_3$ exhibits monoclinic symmetry, as observed in an earlier study [23, 24]. The XRD patterns of Bi$_2$O$_3$@CNTs-20, Bi$_2$O$_3$@CNTs-50, and Bi$_2$O$_3$@CNTs-70 show increased peak intensities at $2\theta = 28.0^\circ$, resulting from the increased Bi$_2$O$_3$ loading [25]. Average crystallite size of Bi$_2$O$_3$ particles was found to be 15.8, 16.8, and 14.9 nm for Bi$_2$O$_3$@CNTs-20, Bi$_2$O$_3$@CNTs-50, and Bi$_2$O$_3$@CNTs-70, respectively, by applying the Debey-Scherer equation: $D = 0.89\lambda/B\cos\theta$, where λ is wavelength, B is full width at half maximum, and θ is Bragg's angle [26].

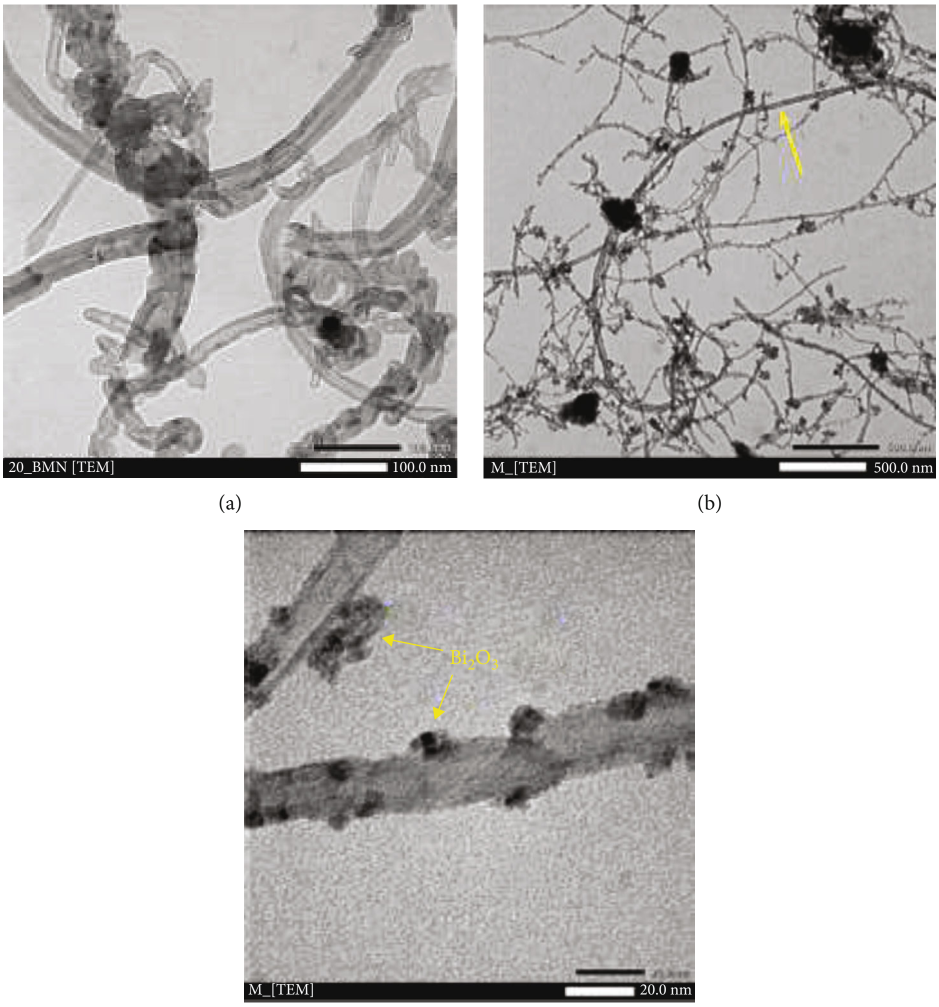

(a)

(b)

(c)

Figure 3: TEM images of (a) CNTs, (b) Bi_2O_3@CNTs-50 at 500 nm scale bar, and (c) Bi_2O_3@CNTs-50 at 20 nm scale bar.

Differences in the microstructures and photon and electron quantum confinements of the electrode materials could be identified from their Raman spectra, as shown in Figure 1(b). Three prominent Raman bands of the CNTs appear at 1325 cm^{-1} (D-band), 1582 cm^{-1} (G-band), and 2656 cm^{-1} (G'-band). The D-band confirms the presence of amorphous carbon owing to structural defects, with strong dispersion leading to double resonance peaks [27, 28]. The G- and G'-bands indicate graphitic rings with sp^2 hybridized C=C bonds [27, 29]. Increased intensity ratios of the D- and G-bands (I_D/I_G) [27] indicate increased microstructural disorder, which is higher for the Bi_2O_3@CNTs than the CNTs. The intensity ratios, $I_{G'}/I_G$, of the CNTs, Bi_2O_3@CNTs-20, Bi_2O_3@CNTs-50, and Bi_2O_3@CNTs-70 (0.75, 0.70, 0.66, and 0.40, respectively) decreased, demonstrating the increased formation of Bi_2O_3 according to the used Bi^{3+} concentrations [27]. The above results could probably be attributed to the attachment of the Bi_2O_3 particles to the CNTs sidewall defects. Finally, the minor D'-band at 1614 cm^{-1} corresponds to the defective graphite structure in the CNTs, typically amorphous hydrogenated carbon (α:C-H) [30]. For Bi_2O_3@CNTs, the dominant vibration band emerged at a low frequency (181 cm^{-1}), ascribed to the displacements of the O atoms in Bi_2O_3 and the overtone vibrations of Bi [31]. This would have probably originated from CNTs. Furthermore, we could not confirm the origin of the relatively weak band at 277 cm^{-1}; however, it is close to the band at 288 cm^{-1} corresponding to multiple regions in the Brillouin zone with a number of photon branches [31].

The SEM micrographs of the electrode materials are shown in Figure 2. Figure 2(a) clearly shows that the individual CNTs exist as tubular fibers with diameters less than 50 nm and are randomly twisted together, generating a three-dimensional network. The presence of Bi_2O_3 particles in the Bi_2O_3@CNTs is obvious owing to the increased utilization of Bi^{3+} in the solutions, as observed in Figures 2(b)–2(d). The Bi_2O_3@CNTs-20 sample presents a sparse distribution of Bi_2O_3 particles (Figure 2(b)). In contrast, Bi_2O_3@CNTs-50 and Bi_2O_3@CNTs-70 indicate widespread, discrete, and relatively homogeneous distributions of Bi_2O_3

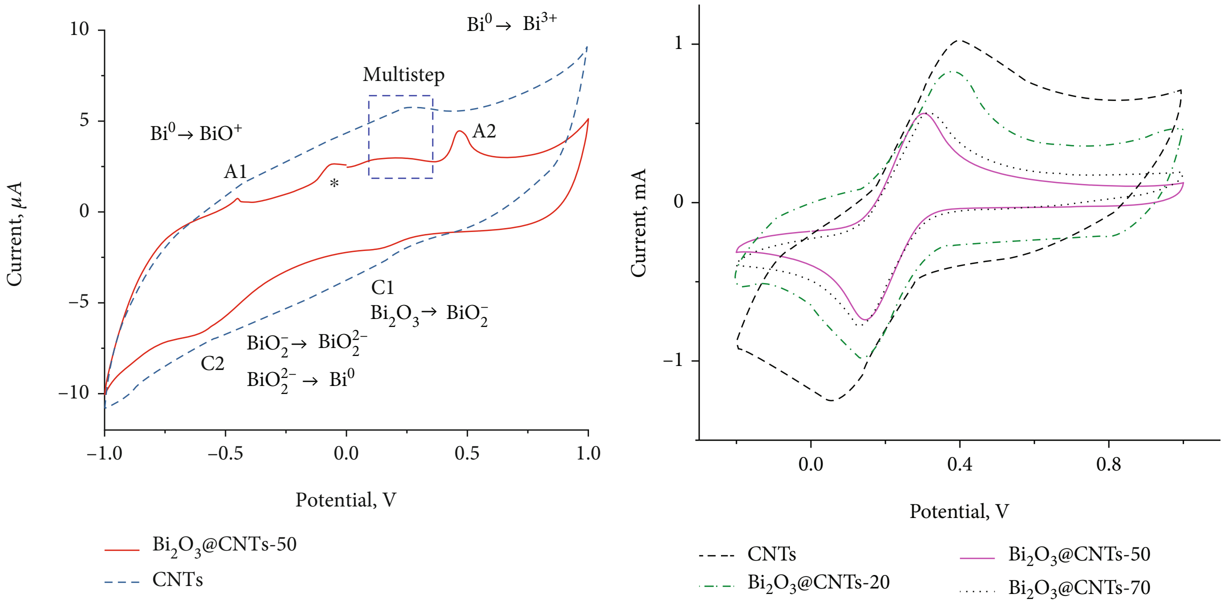

(a)

(b)

Figure 4: Cyclic voltammograms of (a) CNTs and Bi_2O_3@CNTs-50 electrodes in electrolyte without $K_3Fe(CN)_6$ and (b) electrode in electrolyte containing 50 mM $K_3Fe(CN)_6$. Conditions: pH 4 and scan rate of 50 mV/s.

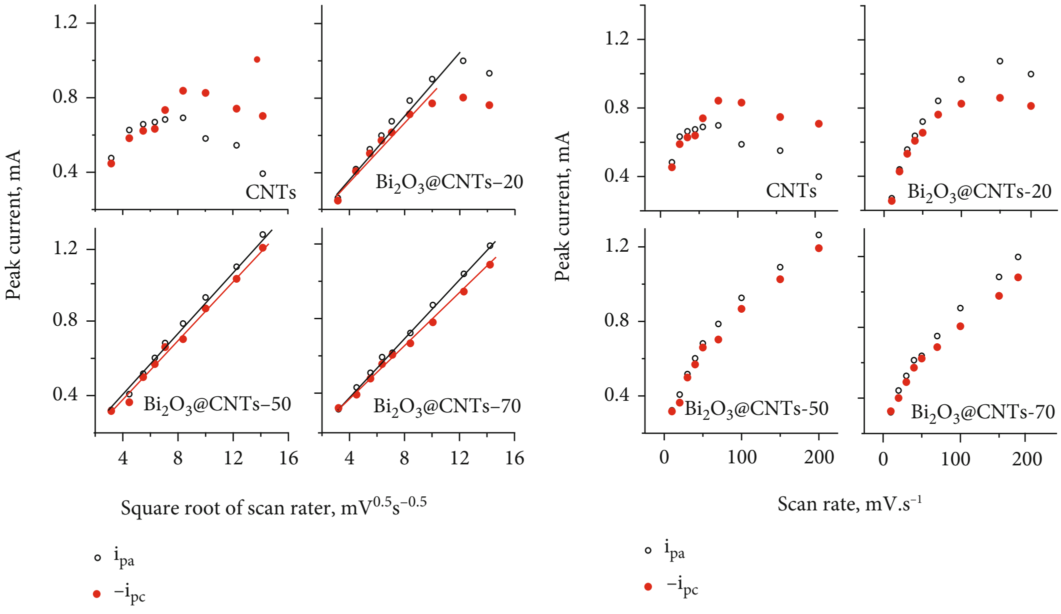

(a)

(b)

Figure 5: Influence of scan rate on peak current determined from CV measurements. Conditions: 50 mM $K_3Fe(CN)_6$ in the electrolyte at pH 4.

particles attached to the CNTs sidewalls. When the used Bi^{3+} quantity exceeds the necessary amount, Bi_2O_3 clusters are formed, as shown in Figure 2(d). This may be disadvantageous to the sensitivity of the Bi_2O_3@CNTs-70 electrode owing to the low electrical conductivity of Bi_2O_3 (~1 S/cm) [32] compared to that of the bulk CNTs (~100 S/cm) [33]. The CNTs serve as skeletons for attaching Bi_2O_3 particles.

TEM analyses of the CNTs and Bi_2O_3@CNTs-50 samples were performed in order to characterize the particle size distribution, and the results are shown in Figure 3. Most of

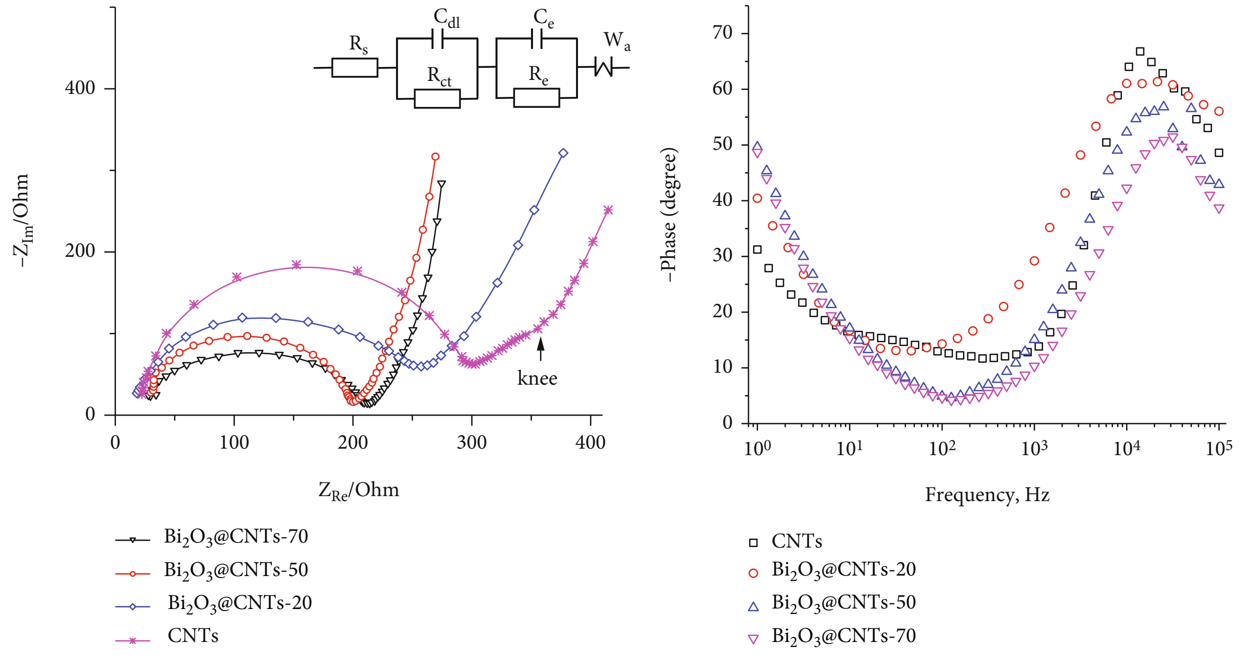

(a)

(b)

FIGURE 6: (a) Nyquist and (b) Bode plots developed from EIS data of the electrodes. Conditions: 50 mM $K_3Fe(CN)_6$ in the electrolyte, pH 4.

TABLE 1: Fe^{2+}/Fe^{3+} peak potentials and currents obtained from CV curves.

	Electrodes			
	CNTs	Bi_2O_3@CNTs-20	Bi_2O_3@CNTs-50	Bi_2O_3@CNTs-70
i_{pa} (mA)	0.613	0.634	0.677	0.649
E_{pa} (V)	0.384	0.373	0.301	0.321
$-i_{pc}$ (mA)	0.736	0.672	0.658	0.675
E_{pc} (V)	0.067	0.143	0.148	0.132

the CNTs are tubular porous structures with nonsmoothed surfaces caused by the defective CNTs sidewalls. Impurities in CNTs did not present through the TEM images (Figure 3(a)) as well as XRD pattern for CNTs (Figure 1(a)). The morphology of Bi_2O_3@CNTs-50 (Figures 3(b) and 3(c)) shows that the Bi_2O_3 particles are discretely attached to the CNTs. The arrow in Figure 3(b) points to a smooth CNT with little or no Bi_2O_3 attached to it. Figure 3(c) shows that Bi_2O_3 nanoparticles are present on the outer walls of the CNTs at defect points but do not enter the hollow channels inside the CNTs, indicating excellent agreement with the Raman spectra analyses. A recent study by Dighole et al. [23] also proved the formation of Bi_2O_3-decorated multiwalled carbon nanotubes via TEM imaging. However, the TEM studies conducted by Dighole et al. did not show the presence of Bi_2O_3 on the outer walls of the CNTs.

3.2. Electrochemical Properties of the Electrodes. The electrochemical characteristics of the electrodes were investigated from CV and EIS measurements, as illustrated in Figures 4–6. The area of the CV curve (Figure 4(a)) of the CNTs electrode is 1.48-folds higher than that of the Bi_2O_3@CNTs-50 electrode, indicating the reduced specific capacitance of the CNTs with attached Bi_2O_3 [34]. This characteristic of the Bi_2O_3@CNTs-50 electrode is advantageous for distinguishing the Faradic current in the analytical signals [35]. The current curves in Figure 4(a) appear as a knob hill at +0.25 V. This may be attributed to the multistep redox reactions between the O atoms in the C–O or/and C=O bond(s) present in the CNTs, although the CNTs were treated at a high temperature [36]. In the CV curve of the Bi_2O_3@CNTs-50 electrode (Figure 4(a)), the small peak C1 at +0.15 V demonstrates the partial reduction of Bi_2O_3 into BiO_2^- ions; peak C2 at −0.61 V corresponds to the successive reduction of BiO_2^- into BiO_2^{2-} and subsequently to Bi^0 [37]. The anodic potential scan results showed that the Bi^0 on the surface Bi_2O_3@CNTs-50 electrode was oxidized to BiO^+ through an active dissolution process [37, 38], resulting in the appearance of peak A1 (Figure 4(a)) at −0.44 V. Peak A2 (+0.48 V) corresponds to the oxidation of Bi^0 to

Table 2: Parameters obtained from EIS data fitting.

	Electrodes			
	CNTs	Bi_2O_3@CNTs-20	Bi_2O_3@CNTs-50	Bi_2O_3@CNTs-70
R_s (Ω)	4.3	14.0	19.3	24.4
C_{dl} (F)	3.3×10^{-4}	3.1×10^{-7}	1.7×10^{-7}	1.5×10^{-7}
R_{ct} (Ω)	6.6	211.2	171.7	156.6
C_e (F)	9.7×10^{-7}	10.2×10^{-4}	7.0×10^{-4}	9.2×10^{-4}
R_e (Ω)	281.7	81.4	58.5	45.4
W_a (Ω)	387.0	266.0	78.4	87.8

Bi^{3+}. The potentials of the anodic peaks (A1 and A2) are higher than those of the cathodic peaks (C2 and C1), as shown in Figure 4(a). This trend, resulting from the change in surface coverage and thickness of the electrode/electrolyte interface (electrical double layer (EDL)), was also observed earlier [39]. The peak (∗) close to 0 V in the CV curve for the Bi_2O_3@CNTs-50 electrode (Figure 4(a)) is similar to that observed in a previous study [40], but it did not appear for Bi_2O_3/Pt [37] and Bi_2O_3/Au [39] electrodes. Notably, BiO^+ was formed and captured on the double layer until saturation under controlled charge transfer and mass diffusion [38]. For porous electrode materials such as CNTs, the double layer is thick and has a high ionic capacity [41], particularly for BiO^+ in the present study, resulting in the peak (∗) because of the discharge in the anodic process.

The CV curve of the ferricyanide system (Fe^{2+}/Fe^{3+}) was used to characterize the influence of Bi_2O_3 on the electrochemical kinetics at the electrodes. CV's wave shapes and sharp redox peaks are evident for the Bi_2O_3@CNTs electrodes as expected (Figure 4(b)). The CV curve of the CNTs electrode (in Figure 4(b)) indicates a higher capacitive current and a more significant peak-to-peak separation (ΔE_p) compared to that of the others, demonstrating a lower electron transfer rate. The Bi_2O_3@CNTs-50 electrode exhibits the lowest anodic peak potential (E_{pa}) and the highest anodic peak current (i_{pa}) among the fabricated electrodes, as observed in Table 1. The peak potential and current are affected by the electrode/electrolyte interface and electrical conductivity of the electrode material [42]. The double layer effects on the interface could have decreased in the presence of Bi_2O_3. According to Figure 4(b) and Table 1, the maximum i_{pa} and minimum ΔE_p are 0.677 mA and 0.153 V, respectively, for the Bi_2O_3@CNTs-50 electrode, indicating optimal electrode performance with contributions from the CNTs and Bi_2O_3 for sensing applications. Additionally, the redox electrochemical reactions of the Fe^{2+}/Fe^{3+} couple on the Bi_2O_3@CNTs-50 electrode exhibited reversibility as the i_{pa}/i_{pc} ratio was close to 1.

The anodic and cathodic peak currents of the Fe^{2+}/Fe^{3+} couple determined from the CV curves of the electrodes as a function of the scan rate (v) from 10 to 200 mV/s are shown in Figure 5. Good linear correlations between the peak currents and square roots of the scan rates ($v^{1/2}$) are observed for the Bi_2O_3@CNTs-50 and Bi_2O_3@CNTs-70 electrodes (Figure 5(a)), indicating that the redox process involves controlled diffusion [43]. However, this behavior is not observed for the CNTs and Bi_2O_3@CNTs-20 electrodes; at low scan rates, the peak current increased with the increasing scan rate for these electrodes, the opposite of what occurred at high scan rates. This trend was also observed in an earlier study [44]. The porous electrode surface generates a complex and thick EDL [45], resulting in a heterogeneous electron transfer rate; therefore, the intensity of the peak current decreases at a high scan rate [46]. However, understanding of this influence is limited in the literature. Consequently, Bi_2O_3 enhanced the electrochemical performance of the electrode, thus proving its potential for analytical applications. Moreover, the poor linear correlations between the peak responses and scan rates are evident in Figure 5(b), verifying that the adsorptive resistance can be neglected [47].

The EIS spectra of the electrodes in Figure 6(a) indicate that the interfacial process is a combination of controlled charge transfer (indicated by semicircles) and controlled mass diffusion (indicated by arcs).

The "knee" in the EIS spectrum of the CNTs electrode (Figure 6(a)) shows the existence of a transition region between charge transfer and mass diffusion [48]. Moreover, the radius of the semicircle is large in the EIS spectrum of the CNTs electrode, indicating the dominance of charge transfer, thereby resulting in the nonlinear relationship between the peak current and the square root of the scan rate (Figure 5(a)). For the Bi_2O_3@CNTs electrodes, the contribution of the charge transfer decreased and that of mass diffusion increased. Steep arcs exceeding 45° at low frequencies indicate the pore narrowing phenomenon on the electrode surface with depth penetration [49]. For porous electrodes, the complex electron transfers occur through the electrolyte, EDL, electrode material itself, and diffusion of the electrolyte onto the electrode [50, 51], represented by the R_s, $(C_{dl}//R_{ct})$, $(C_e//R_e)$, and W_a elements in the equilibrium circuit shown in Figure 6(a). Table 2 presents the parameters obtained from fitting the EIS data to this circuit. The EDL capacitance (C_{dl}) of the Bi_2O_3@CNTs electrode is significantly lower than that of the CNTs one, indicating the planar surface of the Bi_2O_3@CNTs electrode owing to the attachment of Bi_2O_3 particles on the CNTs sidewalls at the defect points. Moreover, the Warburg element (W_a) of the electrode decreased in the presence of Bi_2O_3, proving that Bi_2O_3 contributed toward decreasing the porosity of CNTs, thereby limiting the diffusion of the electrolyte onto the electrode [52]. The enhanced charge transfer in Bi_2O_3@CNTs electrodes is demonstrated by the lower electrical resistance (R_e) when compared to that of the CNTs because of the hybridization reactions between the Bi-$6p^3$

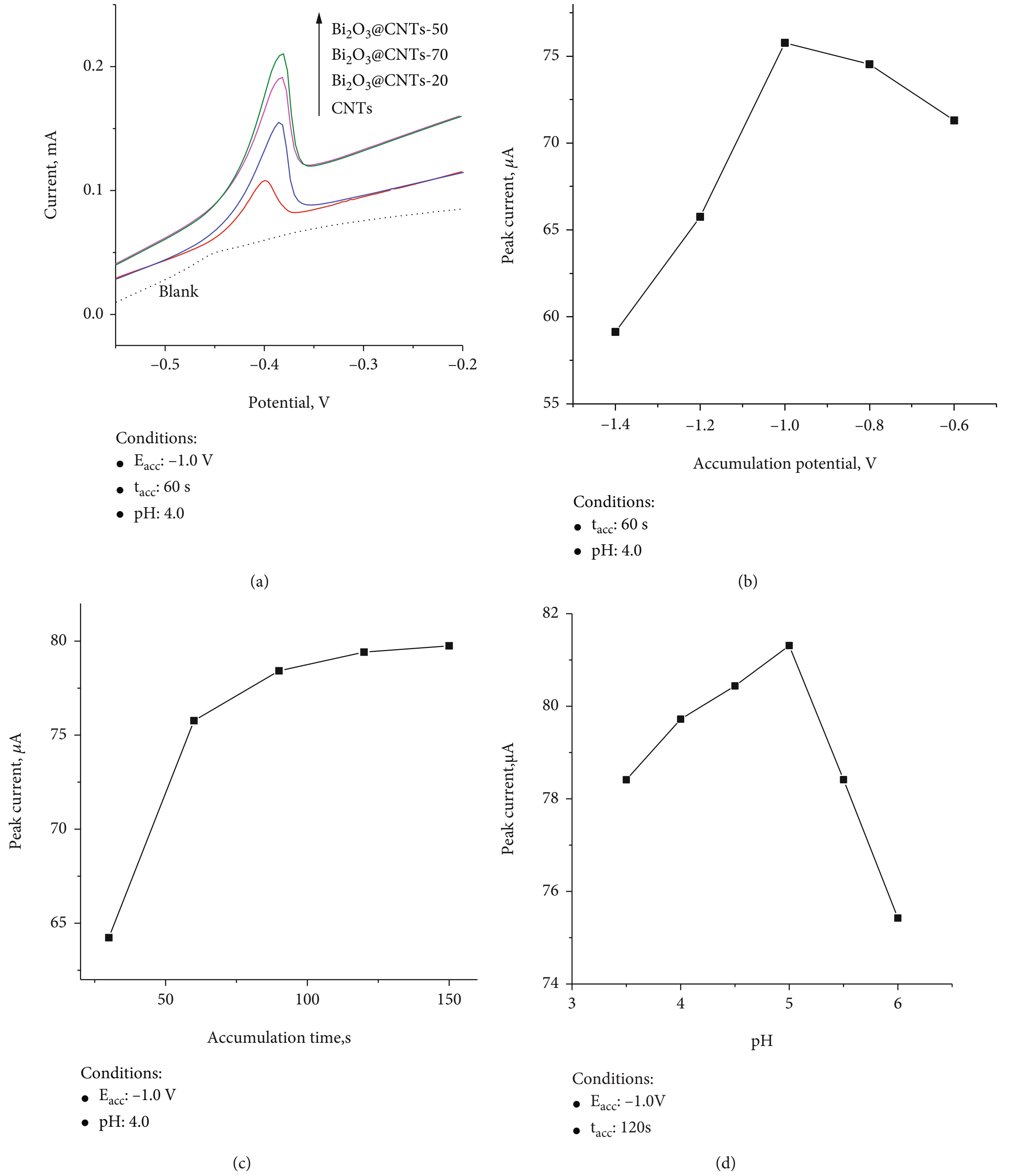

Conditions:

- E_{acc}: −1.0 V
- t_{acc}: 60 s
- pH: 4.0

(a)

Conditions:

- t_{acc}: 60 s
- pH: 4.0

(b)

Conditions:

- E_{acc}: −1.0 V
- pH: 4.0

(c)

Conditions:

- E_{acc}: −1.0V
- t_{acc}: 120s

(d)

Figure 7: (a) Anodic stripping voltammograms for different electrodes and effects of (b) accumulation potential, (c) accumulation time, and (d) pH on Pb^{2+} detection observed for the Bi_2O_3@CNTs-50 electrode. Solution contains 30 μg/L Pb^{2+} and 0.1 M acetate buffer.

and CNT-p^2 orbitals, leading to reduced bandgaps in Bi_2O_3 and CNTs [53]. A similar trend was also observed earlier [44]. However, the capacitance (C_e) of Bi_2O_3@CNTs is higher than that of the CNTs owing to the high permittivity of Bi_2O_3 [54]. The multistep mechanism of the electrochemical process on the electrode surface in the presence of Bi [40] affects the charge transfer resistance (R_{ct}) of the EDL [55] that may have led to a higher R_{ct} of the Bi_2O_3@CNTs electrode than that observed for the CNTs electrode. However, the values of ($R_{ct} + R_e$) for the Bi_2O_3@CNTs electrodes are generally lower than that for the CNTs electrode, indicating the positive effect of Bi_2O_3 on electrical signal conductivity. These results agree with the CV measurements shown in Figure 4(b).

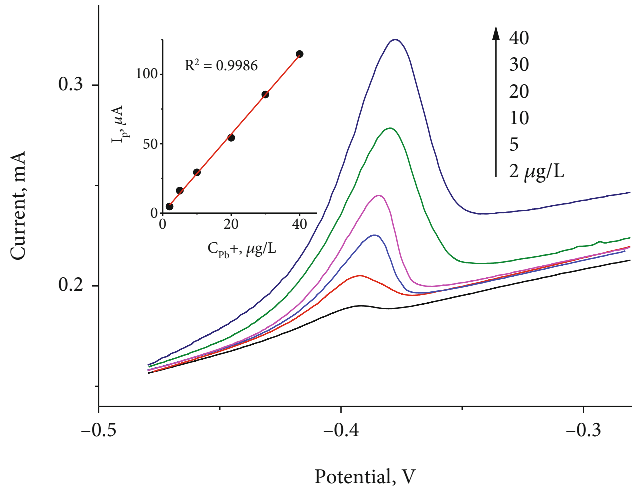

Figure 8: Anodic stripping voltammograms of the Bi_2O_3@CNTs-50 electrode with Pb^{2+} concentration gradient in 0.1 M acetate buffer solution (pH 5.0). Insert: calibration plot. Conditions: $E_{acc} = -1.0\ V$ and $t_{acc} = 120\ s$.

Figure 6(b) shows the frequency-dependent phase angles (Bode plots). The phase angles of the electrodes are higher than −90° at low frequencies, indicating the pseudocapacitive behavior of the electrolyte/electrode interface [56]. Moreover, the broad peaks at high frequencies confirm diffusion resistance in the interfacial process. The higher the peak frequency, the stronger is the effect of controlled diffusion [57]. Consequently, controlled diffusion dominates the redox process of the Fe^{2+}/Fe^{3+} couple at the Bi_2O_3@CNTs electrodes.

3.3. ASV Studies. The electrochemical responses of the different electrodes to Pb^{2+} (Figure 7(a)) were examined via ASV measurements in 0.1 M acetate buffer solution containing 30 μg/L of Pb^{2+}. At an E_{acc} of −0.1 V, Bi_2O_3 was reduced to Bi^0 (indicated in Figure 4(a)), which further enriched Pb by forming Bi-Pb alloys [15]. Consequently, the Bi_2O_3@CNTs electrodes exhibited enhanced Pb^{2+} sensing properties compared to those of the CNTs electrode, as indicated by their improved anodic peak currents. The peak potential was approximately −0.40 V for the CNTs electrode, whereas it was approximately −3.83 V for the Bi_2O_3@CNTs electrodes. This positive shift reveals a more complex reduction of Pb^0 because of Bi-Pb alloy formation [15] on the Bi_2O_3@CNTs electrodes than on the CNTs electrode, indicating differences in the interaction mechanism between Pb^{2+} and the CNTs and between Pb^{2+} and Bi_2O_3@CNTs electrode surfaces [58]. The sensitivity for Pb^{2+} detection increases in the following order: CNTs, Bi_2O_3@CNTs-20, Bi_2O_3@CNTs-70, and Bi_2O_3@CNTs-50 electrodes. Therefore, the Bi_2O_3@CNTs-50 electrode is a favorable candidate for Pb^{2+} detection applications.

Important parameters of the LSASV technique (E_{acc}, t_{acc}, and pH) were considered to optimize Pb^{2+} detection using the Bi_2O_3@CNTs-50 electrode. Figures 7(b)–7(d) show the peak currents obtained from the ASV measurements under different conditions.

The CV measurements presented in Figure 4(a) indicate that Bi^{3+} in Bi_2O_3 is reduced to Bi^0 at −0.61 V, revealing the upper E_{acc} limit for electrochemical analyses involving Pb^{2+}. Figure 7(b) shows that the stripping response of Pb^{2+} depends on the accumulation potential in the interval from −1.4 V to −0.6 V. The Pb oxidative peak signal increases with a negative shift of the E_{acc} from −0.6 V to −1.0 V resulting from the enhanced microstructural parameters of the deposited Bi^0 particles such as their size and distribution [59], thus improving the Pb-Bi alloy formation [60]. However, the hydrogen evolution reaction on the electrode surface begins to occur at −1.2 V in an acidic electrolyte [16], which could have prevented Pb^{2+} deposition and damaged the Bi^0 film. This led to a substantial decrease in the stripping response at a high negative E_{acc}. Consequently, $E_{acc} = -1.0$ V was considered the optimum accumulation potential and applied in the accumulation time (t_{acc}) studies. Figure 7(c) presents the effects of different t_{acc} values, namely, 30, 60, 90, 120, and 150 s, on the stripping signals. With a prolonged t_{acc}, the amount of Pb deposited on the electrode surface increased until saturation, resulting in a rapidly increasing peak current with t_{acc} up to 120 s and then tending to remain constant at a longer t_{acc}. Thus, $t_{acc} = 120$ s was chosen as the suitable accumulation time for subsequent experiments. As depicted in Figure 7(d), the pH has a significant influence on the peak signal. At low pH, the stripping current decreases due to protonation of the CNTs structure with the increasing bandgap [61]. Moreover, the potential for hydrogen evolution shifts to more positive values at low pH; thus, the peak current is low at low pH. In contrast, at high pH, Pb^{2+} and intermediate forms of Bi could be converted to insoluble hydroxide complexes [62], leading to decreasing peak currents with increasing pH. Figure 7(d) shows that the optimum sensitivity of the electrodes for Pb^{2+} is at pH = 5.0.

To evaluate the applicability of the Bi_2O_3@CNTs-50 electrode for Pb^{2+} detection, the relationships of current responses with Pb^{2+} concentrations were determined from the electrochemical measurements using the LSASV technique using the following optimal parameters: $E_{acc} = -1.0$ V, $t_{acc} = 120$ s, and pH = 5.0. The obtained voltammograms are presented in Figure 8, along with the calibration plot of Pb^{2+} in the range of 2–40 μg/L (in the insert). The peak current is directly proportional to the Pb^{2+} concentration according to the following linear regression equation: $i(\mu A) = 2.842 \times C_{Pb^{2+}}(\mu g/L) + 0.07$ (correlation coefficient $R^2 = 0.9986$). The limit of detection (LOD) was 3.44 μg/L according to the 3σ criteria ($N = 6$). Table 3 compares the obtained LOD and sensitivity with those in previous reports, proving the applicability of the fabricated Bi_2O_3@CNTs electrodes for Pb^{2+} detection.

3.4. Application to River Water Media. Water from the Saigon River was collected, filtered through a 0.45 μm membrane, and sonicated for ICP-MS and ASV measurements. Because the Pb^{2+} concentration in the sample was lower than the LOD of the ICP-MS method, this natural water was used as the medium for preparing the ASV analytical solution containing 5 μg/L Pb^{2+}, 0.1 M KCl, and 0.1 M acetate buffer (pH 4.0). Under the optimal conditions, the

Table 3: Performance comparison of Bi_2O_3-modified electrodes for Pb^{2+} detection.

Electrode	Modification method	LOD (μg/L)	Sensitivity (μA/(μg/L))	Method	Ref.
Bi_2O_3-CS/GCPE	Surface dropping	30.1	0.045	DPASV	[63]
Bi_2O_3/SPE	Bulk modification	20.0	0.011	DPASV	[64]
Bi_2O_3/SPE	Bulk modification	10.0	—	DPASV	[65]
Bi_2O_3/SPE	Bulk modification	8.0	1.050	CCSCP	[66]
Bi_2O_3/SPE	Bulk modification	5.0	0.074	SWASV	[67]
Bi_2O_3/SPE	Surface modification	2.3	2.960	SWASV	[16]
Bi_2O_3@CNTs	Attachment	3.4	2.842	LSASV	This work

GCPE: glassy carbon paste electrode; CS: chitosan; SPE: screen-printed electrode; SWASV: square wave anodic stripping voltammetry; DPASV: different pulse anodic stripping voltammetry; CCSCP: constant current stripping chronopotentiometry.

Table 4: Concentrations of Pb^{2+} determined in river water media.

No.	1	2	3	4	5
Pb^{2+} (μg/L)	4.3	4.7	4.7	4.4	4.8

ASV measurement using the Bi_2O_3@CNTs-50 electrode was repeated five times (shown in Table 4), revealing a Pb^{2+} concentration of $4.58 \pm 0.22\,\mu$g/L with a 9.7% standard error. These results prove the excellent applicability of the electrode for Pb^{2+} determination at the trace level.

4. Conclusion

The successful attachment of Bi_2O_3 particles at the defect points on the outer walls of the CNTs produced the Bi_2O_3@CNTs materials with advantageous properties for electrochemical analytical applications. The interfacial process on the Bi_2O_3@CNTs electrodes was predominantly controlled mass diffusion instead of controlled charge transfer observed for the CNTs electrode. The ASV studies using the fabricated electrodes indicated the superior sensitivity of the Bi_2O_3@CNTs electrodes for Pb^{2+} detection compared to that of the CNTs electrode. The optimal parameters for Pb^{2+} detection using the LSASV technique, namely, the accumulation potential, accumulation time, and pH of the solution, were determined. The obtained detection limit and sensitivity from the Pb^{2+} calibration curve revealed the excellent applicability of the Bi_2O_3@CNTs electrodes for detecting heavy metal ions. In the future, the interaction mechanisms between Bi_2O_3 and CNTs and other applications of the Bi_2O_3@CNTs electrodes will be investigated.

Data Availability

The experimental data used to support the findings of this study are included within the article.

Conflicts of Interest

The authors declare that they have no conflicts of interest.

References

[1] A. L. Wani, A. Ara, and J. A. Usmani, "Lead toxicity: a review," *Interdisciplinary Toxicology*, vol. 8, no. 2, pp. 55–64, 2015.

[2] A. J. Borrill, N. E. Reily, and J. V. Macpherson, "Addressing the practicalities of anodic stripping voltammetry for heavy metal detection: a tutorial review," *Analyst*, vol. 144, no. 23, pp. 6834–6849, 2019.

[3] M. Oliveira Salles, A. . P. Ruas de Souza, J. Naozuka, P. . V. de Oliveira, and M. Bertotti, "Bismuth modified gold microelectrode for Pb(II) determination in wine using alkaline medium," *Electroanalysis*, vol. 21, no. 12, pp. 1439–1442, 2009.

[4] A. García-Miranda Ferrari, P. Carrington, S. J. Rowley-Neale, and C. E. Banks, "Recent advances in portable heavy metal electrochemical sensing platforms," *Environmental Science: Water Research & Technology*, vol. 6, no. 10, pp. 2676–2690, 2020.

[5] J. A. Barón-Jaimez, J. L. Marulanda-Arévalo, and J. J. Barba-Ortega, "Electrodes friendly with the environment for detect heavy metal," *Dyna*, vol. 81, no. 187, pp. 122–128, 2014.

[6] P. Zuman, "Role of mercury Electrodes in contemporary analytical chemistry," *Electroanalysis: An International Journal Devoted to Fundamental and Practical Aspects of Electroanalysis*, vol. 12, no. 15, pp. 1187–1194, 2000.

[7] A. Vimala and C. Vedhi, "Electrochemical sensors for heavy metals detection in *Gracilaria corticata* using multiwalled carbon nanotubes modified glassy carbon electrode," *Journal of Analytical Chemistry*, vol. 74, no. 3, pp. 276–285, 2019.

[8] M. Pumera, A. Ambrosi, A. Bonanni, E. L. K. Chng, and H. L. Poh, "Graphene for electrochemical sensing and biosensing," *TrAC Trends in Analytical Chemistry*, vol. 29, no. 9, pp. 954–965, 2010.

[9] X. Xuan, M. F. Hossain, and J. Y. Park, "A fully integrated and miniaturized heavy-metal-detection sensor based on micro-patterned reduced graphene oxide," *Scientific Reports*, vol. 6, no. 1, article 33125, 2016.

[10] J. Wu, Z. Xu, X. Wang et al., "Cadmium-sensitive measurement using a nano-copper-enhanced carbon fiber electrode," *Sensors*, vol. 19, no. 22, p. 4901, 2019.

[11] J. Manjunatha, "A new electrochemical sensor based on modified carbon nanotube-graphite mixture paste electrode for voltammetric determination of resorcinol," *Asian Journal of Pharmaceutical and Clinical Research*, vol. 10, no. 12, pp. 295–300, 2017.

[12] G. E. Uwaya and O. E. Fayemi, "Electrochemical detection of choline at f-MWCNT/Fe_3O_4 nanocomposite modified glassy

carbon electrode," *Materials Research Express*, vol. 8, no. 5, article 055403, 2021.

[13] C. Hu and S. Hu, "Carbon Nanotube-Based Electrochemical Sensors: Principles and Applications in Biomedical Systems," *Nanomaterials for Chemical Sensing Technologies*, vol. 2009, article 187615, pp. 1–40, 2009.

[14] L. Pujol, D. Evrard, K. Groenen-Serrano, M. Freyssinier, A. Ruffien-Cizsak, and P. Gros, "Electrochemical sensors and devices for heavy metals assay in water: the French groups' contribution," *Frontiers in Chemistry*, vol. 2, 2014.

[15] J. Wang, "Stripping analysis at bismuth electrodes: a review," *Electroanalysis*, vol. 17, no. 15-16, pp. 1341–1346, 2005.

[16] G. Hwang, W. Han, J. Park, and S. Kang, "Determination of trace metals by anodic stripping voltammetry using a bismuth-modified carbon nanotube electrode," *Talanta*, vol. 76, no. 2, pp. 301–308, 2008.

[17] N. Serrano, A. Alberich, J. M. Díaz-Cruz, C. Ariño, and M. Esteban, "Coating methods, modifiers and applications of bismuth screen-printed electrodes," *TrAC Trends in Analytical Chemistry*, vol. 46, pp. 15–29, 2013.

[18] A. Economou, "Screen-printed electrodes modified with "green" metals for electrochemical stripping analysis of toxic Elements," *Sensors*, vol. 18, no. 4, p. 1032, 2018.

[19] A. T. Kuhn and C. Y. Chan, "pH changes at near-electrode surfaces," *Journal of Applied Electrochemistry*, vol. 13, no. 2, pp. 189–207, 1983.

[20] C. Dossi, D. Monticelli, A. Pozzi, and S. Recchia, "Exploiting chemistry to improve performance of screen-printed, bismuth film electrodes (SP-BiFE)," *Biosensors (Basel)*, vol. 6, no. 3, p. 38, 2016.

[21] R. Das, S. B. A. Hamid, M. E. Ali, S. Ramakrishna, and W. Yongzhi, "Carbon nanotubes characterization by X-ray powder diffraction – a review," *Current Nanoscience*, vol. 11, no. 1, pp. 23–35, 2015.

[22] L. Xu, Y. Zhang, X. Zhang et al., "Designed synthesis of tunable amorphous carbon nanotubes (a-CNTs) by a novel route and their oxidation resistance properties," *Bulletin of Materials Science*, vol. 37, no. 6, pp. 1397–1402, 2014.

[23] R. P. Dighole, A. V. Munde, B. B. Mulik, and B. R. Sathe, "Bi_2O_3 nanoparticles decorated carbon Nanotube: an Effective nanoelectrode for Enhanced electrocatalytic 4-nitrophenol reduction," *Frontiers in Chemistry*, vol. 8, 2020.

[24] A. P. Periasamy, S. Yang, and S.-M. Chen, "Preparation and characterization of bismuth oxide nanoparticles-multiwalled carbon nanotube composite for the development of horseradish peroxidase based H_2O_2 biosensor," *Talanta*, vol. 87, pp. 15–23, 2011.

[25] Z. Jian and W. Hejing, "The physical meanings of 5 basic parameters for an X-ray diffraction peak and their application," *Chinese Journal of Geochemistry*, vol. 22, no. 1, pp. 38–44, 2003.

[26] R. I. Jibrael and M. K. A. Mohammed, "Production of graphene powder by electrochemical exfoliation of graphite electrodes immersed in aqueous solution," *Optik*, vol. 127, no. 16, pp. 6384–6389, 2016.

[27] L. Bokobza, J. L. Bruneel, and M. Couzi, "Raman spectra of carbon-based materials (from graphite to carbon black) and of some silicone composites," *C—Journal of Carbon Research*, vol. 1, no. 1, pp. 77–94, 2015.

[28] D. S. Ahmed, M. K. A. Mohammed, and M. R. Mohammad, "Sol–gel synthesis of Ag-doped titania-coated carbon nanotubes and study their biomedical applications," *Chemical Papers*, vol. 74, no. 1, pp. 197–208, 2020.

[29] M. Zdrojek, W. Gebicki, C. Jastrzebski, T. Melin, and A. Huczko, "Studies of multiwall carbon nanotubes using Raman spectroscopy and atomic force microscopy," *Solid State Phenomena*, vol. 99-100, pp. 265–268, 2004.

[30] F. K. Tung, M. Yoshimura, and K. Ueda, "Direct fabrication of carbon nanotubes STM tips by liquid catalyst-assisted microwave plasma-enhanced chemical vapor deposition," *Journal of Nanomaterials*, vol. 2009, Article ID 612549, 5 pages, 2009.

[31] J. S. Lannin, J. M. Calleja, and M. Cardona, "Second-order Raman scattering in the group-V_b semimetals: Bi, Sb, and As," *Physical Review B*, vol. 12, no. 2, pp. 585–593, 1975.

[32] R. Mandfield, "The electrical properties of bismuth oxide," *Proceedings of the Physical Society. Section B*, vol. 62, no. 8, pp. 476–483, 1949.

[33] H. L. Zhang, J. F. Li, B. P. Zhang, K. F. Yao, W. S. Liu, and H. Wang, "Electrical and thermal properties of carbon nanotube bulk materials: experimental studies for the 328–958K temperature range," *Physical Review B*, vol. 75, no. 20, article 205407, 2007.

[34] M. Nawwar, R. Poon, R. Chen, R. P. Sahu, I. K. Puri, and I. Zhitomirsky, "High areal capacitance of Fe_3O_4-decorated carbon nanotubes for supercapacitor electrodes," *Carbon Energy*, vol. 1, no. 1, pp. 124–133, 2019.

[35] F. Scholz, "Voltammetric techniques of analysis: the essentials," *ChemTexts*, vol. 1, no. 4, article 17, 2015.

[36] M. T. Caccamo, G. Mavilia, and S. Magazù, "Thermal investigations on carbon nanotubes by spectroscopic techniques," *Applied Sciences*, vol. 10, no. 22, p. 8159, 2020.

[37] V. Vivier, A. Régis, G. Sagon, J. Y. Nedelec, L. T. Yu, and C. Cachet-Vivier, "Cyclic voltammetry study of bismuth oxide Bi_2O_3 powder by means of a cavity microelectrode coupled with Raman microspectrometry," *Electrochimica Acta*, vol. 46, no. 6, pp. 907–914, 2001.

[38] W. S. Li, X. M. Long, J. H. Yan, J. M. Nan, H. Y. Chen, and Y. M. Wu, "Electrochemical behaviour of bismuth in sulfuric acid solution," *Journal of Power Sources*, vol. 158, no. 2, pp. 1096–1101, 2006.

[39] C. Lee, S. Jeong, N. Myung, and K. Rajeshwar, "Preparation of Au-Bi_2O_3 Nanocomposite by anodic electrodeposition combined with galvanic replacement," *Journal of The Electrochemical Society*, vol. 161, no. 10, pp. D499–D503, 2014.

[40] T. T. P. Nguyen, X. G. Trinh, and D. T. T. Uyen, "Using electrode made of carbon nanotubes and bismuth oxide for the determination of metal concentration by anodic stripping voltammetry," *Journal of Chemistry*, vol. 2019, Article ID 6170967, 7 pages, 2019.

[41] T. Trunzer, T. Stummvoll, M. Porzenheim, P. Fraga-García, and S. Berensmeier, "A carbon nanotube packed bed electrode for small molecule electrosorption: an electrochemical and chromatographic approach for process description," *Applied Sciences*, vol. 10, no. 3, p. 1133, 2020.

[42] Y. Choudhary, L. Jothi, and G. Nageswaran, "Electrochemical characterization," in *Spectroscopic Methods for Nanomaterials Characterization*, S. Thomas, R. Thomas, A. Zachariah, and R. Mishra, Eds., pp. 19–54, Elsevier Inc, U.S., 2017.

[43] J. E. B. Randles, "A cathode ray polarograph. Part II.—the current-voltage curves," *Transactions of the Faraday Society*, vol. 44, pp. 327–338, 1948.

[44] Y. Suzuki, Y. Fukunaka, and T. Goto, "Interfacial phenomena associated with Li electrodeposition on liquid Ga substrates in propylene carbonate," *Electrochemistry Communications*, vol. 100, pp. 20–25, 2019.

[45] H. Tao, C. Lian, and H. Liu, "Multiscale modeling of electrolytes in porous electrode: from equilibrium structure to non-equilibrium transport," *Green Energy & Environment*, vol. 5, no. 3, pp. 303–321, 2020.

[46] S. Sarker, P. Chaturvedi, L. Yan et al., "Synergistic effect of iron diselenide decorated multi-walled carbon nanotubes for enhanced heterogeneous electron transfer and electrochemical hydrogen evolution," *Electrochimica Acta*, vol. 270, pp. 138–146, 2018.

[47] N. Elgrishi, K. J. Rountree, B. D. McCarthy, E. S. Rountree, T. T. Eisenhart, and J. L. Dempsey, "A practical beginner's guide to cyclic voltammetry," *Journal of Chemical Education*, vol. 95, no. 2, pp. 197–206, 2018.

[48] T. Q. Nguyen and C. Breitkopf, "Determination of diffusion coefficients using impedance spectroscopy data," *Journal of The Electrochemical Society*, vol. 165, no. 14, pp. E826–E831, 2018.

[49] S. J. Cooper, A. Bertei, D. P. Finegan, and N. P. Brandon, "Simulated impedance of diffusion in porous media," *Electrochimica Acta*, vol. 251, pp. 681–689, 2017.

[50] W. Kwon, J. M. Kim, and S. W. Rhee, "A new equivalent circuit model for porous carbon electrodes in charge transfer reaction of iodide/triiodide redox couples," *Electrochimica Acta*, vol. 68, pp. 110–113, 2012.

[51] N. F. Sylla, N. M. Ndiaye, B. D. Ngom et al., "Effect of porosity enhancing agents on the electrochemical performance of high-energy ultracapacitor electrodes derived from peanut shell waste," *Scientific Reports*, vol. 9, no. 1, article 13673, 2019.

[52] R. Attias, B. Dlugatch, M. S. Chae, Y. Goffer, and D. Aurbach, "Changes in the interfacial charge-transfer resistance of Mg metal electrodes, measured by dynamic electrochemical impedance spectroscopy," *Electrochemistry Communications*, vol. 124, article 106952, 2021.

[53] L. W. Tack, M. A. Azam, and R. N. A. R. Seman, "Structural and electronic properties of transition metal oxides attached to a single-walled CNT as a lithium-ion battery electrode: a first-principles study," *Journal of Physical Chemistry A*, vol. 121, no. 13, pp. 2636–2642, 2017.

[54] S. Sharma, S. K. Mehta, A. O. Ibhadon, and S. K. Kansal, "Fabrication of novel carbon quantum dots modified bismuth oxide (α-Bi_2O_3/C-dots): material properties and catalytic applications," *Journal of Colloid and Interface Science*, vol. 533, pp. 227–237, 2019.

[55] D. Qu, G. Wang, J. Kafle et al., "Electrochemical impedance and its applications in energy-storage systems," *Small Methods*, vol. 2, no. 8, article 1700342, 2018.

[56] R. Manikandan, C. J. Raj, M. Rajesh, B. C. Kim, J. Y. Sim, and K. H. Yu, "Electrochemical behaviour of lithium, sodium and potassium ion electrolytes in a $Na_{0.33}V_2O_5$ Symmetric pseudocapacitor with high performance and high cyclic stability," *ChemElectroChem*, vol. 5, no. 1, pp. 101–111, 2018.

[57] K. Koteshwara Reddy, M. Satyanarayana, K. Yugender Goud, K. Vengatajalabathy Gobi, and H. Kim, "Carbon nanotube ensembled hybrid nanocomposite electrode for direct electrochemical detection of epinephrine in pharmaceutical tablets and urine," *Materials Science and Engineering C*, vol. 79, pp. 93–99, 2017.

[58] X. Xie, T. Gan, D. Sun, and K. Wu, "Application of multi-walled carbon nanotubes/nafion composite film in electrochemical determination of Pb^{2+}," *Fullerenes, Nanotubes, and Carbon Nanostructures*, vol. 16, no. 2, pp. 103–113, 2008.

[59] A. Królicka and A. Bobrowski, "Bismuth film electrode for adsorptive stripping voltammetry - electrochemical and microscopic study," *Electrochemistry Communications*, vol. 6, no. 2, pp. 99–104, 2004.

[60] L. T. Tufa, K. Siraj, and T. R. Soreta, "Electrochemical determination of lead using bismuth modified glassy carbon electrode," *Russian Journal of Electrochemistry*, vol. 49, no. 1, pp. 59–66, 2013.

[61] M. S. Strano, C. B. Huffman, V. C. Moore et al., "Reversible, band-gap-selective protonation of single-walled carbon nanotubes in solution," *Journal of Physical Chemistry B*, vol. 107, no. 29, pp. 6979–6985, 2003.

[62] S. Lee, J. Oh, D. Kim, and Y. Piao, "A sensitive electrochemical sensor using an iron oxide/graphene composite for the simultaneous detection of heavy metal ions," *Talanta*, vol. 160, pp. 528–536, 2016.

[63] C. Hao, Y. Shen, J. Shen et al., "A glassy carbon electrode modified with bismuth oxide nanoparticles and chitosan as a sensor for Pb(II) and Cd(II)," *Microchimica Acta*, vol. 183, no. 6, pp. 1823–1830, 2016.

[64] J. C. Quintana, F. Arduini, A. Amine et al., "Part I: A comparative study of bismuth-modified screen-printed electrodes for lead detection," *Analytica Chimica Acta*, vol. 707, no. 1-2, pp. 171–177, 2011.

[65] R. Pauliukaite, R. Metelka, I. Švancara et al., "Screen-printed carbon electrodes bulk-modified with Bi_2O_3 or Sb_2O_3 for trace determinations of some trace metals," *Scientific Papers of the University of Pardubic. Series A*, vol. 10, pp. 47–58, 2005.

[66] R. O. Kadara and I. E. Tothill, "Development of disposable bulk-modified screen-printed electrode based on bismuth oxide for stripping chronopotentiometric analysis of lead (II) and cadmium (II) in soil and water samples," *Analytica Chimica Acta*, vol. 623, no. 1, pp. 76–81, 2008.

[67] R. O. Kadara, N. Jenkinson, and C. E. Banks, "Disposable bismuth oxide screen printed electrodes for the high throughput screening of heavy metals," *Electroanalysis*, vol. 21, no. 22, pp. 2410–2414, 2009.